Supplementary Information

S1 Alternative Costs of Immunity

While autoimmunity represents one class of costs that may be associated with prokaryotic immune systems (i.e. lethality via an additional death term), other cost structures exist that may be applied to growth. Immune host may either suffer from reduced resource affinity (z) or maximal growth rate (v). Thus we can write the chemostat system with resources:

$$\dot{R} = w(A - R) - \frac{evR}{z + R}(D + U) \tag{1}$$

defended host:

$$\dot{D} = D\left(\frac{v_d R}{z_d + R} - \delta\phi_d P - \alpha - \mu - w\right), \tag{2}$$

undefended host:

$$\dot{U} = U\left(\frac{v_u R}{z_u + R} - \delta\phi_u P - w\right) + \mu D, \tag{3}$$

and phage:

$$\dot{P} = P\left(\delta U(\phi_u\beta - 1) + \delta D(\phi_d\beta - 1) - w\right), \tag{4}$$

where we let

$$z_d = c_z z_u \tag{5}$$

and

$$v_d = \frac{v_u}{c_v}. \tag{6}$$

so that the resource affinity penalty, c_z, and growth rate penalty, c_v, describe the costs applied to each aspect of host population growth respectively. It is possible that alternative cost regimes are more capable of producing robust coexistence under realistic parameter ranges than is autoimmunity (α).

Both alternative cost regimes can produce stable coexistence (Fig. S1), although they are applied to a nonlinear term in the growth equations and thus behave differently than autoimmunity (Fig. S2). We see that under realistic initial conditions immune loss can produce coexistence over a wider range of parameter space than the other mechanisms, but all can do so over some range and the range of values for μ and α are not easily comparable with the range for c_z and c_v (Fig. S3). All mechanisms can produce coexistence with initial conditions perturbed away from the equilibrium condition (Figs. S4-7), but only immune loss reliably produces coexistence over any part of parameter space when very large perturbations to the system occur (on the order of those expected with serial dilution; Fig. S7). We also note that the condition we call coexistence in Figs. S4-7 is that both immune hosts and phages are present at 80 days at a level likely to be detected experimentally (density of 100/mL) which can be taken as the most general requirement for coexistence. If we observe the distribution of outcomes of these simulations in Fig. S8 we see that growth rate and resource affinity costs tend to produce coexistence regimes that are dominated by susceptible hosts even with more mild perturbations (though still severe).

S2 Parameter Values

For both our analytical and simulation models we attempt to constrain parameter values within realistic ranges where possible. Resource uptake parameters (e, v, z) and burst size (β) are taken from Levin et al. (2013), although they are rough estimates in some cases. We let $\delta = 10^{-8}$ be our base value for the rate of adsorption. Levin et al. (2013) fit a model to data to estimate a value of $\delta = 10^{-7}$, but they also incorporate a lag time, which we approximate by lowering δ tenfold.

Simulation Parameters

The rate of loss of functionality in the CRISPR immune system of *S. epidermidis* has been shown to fall in the range $10^{-4} - 10^{-3}$ losses per individual per generation (Jiang *et al.*, 2013). We choose to use a value in the middle of this range ($\mu_L = 5 \times 10^{-4}$) for our simulations. Similarly, based on the fact that there appears to be no self vs. non-self recognition in the CRISPR system of *S. thermophilus* (Wei *et al.*, 2015), and that the genome of S. thermophilus is roughly 50 times the size of its lytic phage 2972 (Bolotin *et al.*, 2005; Lévesque *et al.*, 2005), the rate of incorporation of a self-spacer by the CRISPR system should be approximately 50 times the spacer acquisition rate per adsorbed phage. Assuming that incorporation of a self-spacer is instantaneously toxic and leads to unavoidable cell death, we can take this value as our rate of autoimmunity ($\alpha = 50\mu_b$). This gives us a value on the high end of possible α values, as it is possible that there is self recognition that has not been observed experimentally or that the action of autoimmunity can be delayed or avoided through spacer loss or corruption, as has been found in some experiments (Jiang *et al.*, 2013; Paez-Espino *et al.*, 2013).

We set $n_s = 10$ due to computational constraints, as small increases in cassette length lead to a large increase in computational time. The experiments we compare our models to saw small expansions of the CRISPR cassette (2-3 spacers) and our system reaches either a phage-cleared or stable coexistence state where coevolution is halted well before host have obtained the complete set of spacers. While the phage genome has many protospacers (200+), in the *S. thermophilus*-phage 2972 system the large majority of spacers come from a small subset of possible protospacers on the phage genome (~ 30), and thus our limited protospacer set may be an appropriate approximation of reality (Paez-Espino *et al.*, 2013). Our value for the cost per PAM mutation (c) is set arbitrarily, but is linked to the value we choose for n_s. Our results are robust to the value of this parameter (Fig. S17).

Childs et al. (2012) uses a value of $\mu_p = 5 \times 10^{-7}$ for the protospacer mutation rate in their model of CRISPR-phage coevolution. We choose to introduce newly mutated strains at a population size of 100 individuals to eliminate the effects of drift in our model and thus speed up our simulations, which requires a corresponding decrease in the mutation rate. Additionally, we choose to consider PAM mutations only, and since the PAM region is considerably shorter than the protospacer itself, this also warrants a decrease in mutation rate. Thus we reduce their parameter estimate tenfold for use in our simulations ($\mu_p = 5 \times 10^{-8}$). Similarly we reduce previous estimates of the spacer acquisition rate ($\mu_b = 10^{-6}$) fivefold to account for our introduction of novel strains at a higher population size (Barrangou *et al.*, 2007; Childs *et al.*, 2012; Deveau *et al.*, 2008; Horvath *et al.*, 2008; Levin *et al.*, 2013).

We use an initial multiplicity of infection (MOI) of 1 phage per host corresponding to experimental values. We simulated outcomes with an initial MOI of 10 to confirm robustness to initial conditions (Fig. S20), as seen in previous experimental work (Paez-Espino *et al.*, 2015). Burst size

(β) estimates for phage are imprecise. We ran additional simulations at high and low burst sizes to confirm that our qualitative results are robust to changes in this parameter (Fig. S21).

Varying adsorption

Because we do not have a good estimate of the rate of adsorption in this system (Levin *et al.*, 2013), and because we choose to depress our adsorption rate as a compensation for the lack of latent period in our models, we explore the response of our results to large variations in δ (Fig. S14, S18).

S3 Analysis and Simulation Methods

Analysis

W found equilibria of our analytical model using Wolfram Mathematica (Version 11.0, Wolfram Research Inc., Champaign, IL, 2016). We assessed stability by linearizing the system around each equilibrium point via the Jacobian. We performed robustness analysis by solving our system numerically using a variable order method for stiff systems (MATLAB 9.0, The MathWorks Inc., Natick, MA, 2016; `ode15s`) at 80 days from inital conditions described in Main Text Fig. 1.

Simulations

We solve our system numerically using a variable order method for stiff systems (MATLAB 9.0, The MathWorks Inc., Natick, MA, 2016; `ode15s`), pausing the solver to add strains due to spacer acquisition and PAM mutation events, and to perform serial dilutions at 24 hour intervals. When we reach a serial dilution the resource concentration is reset to its initial value and all populations are reduced by a factor of 100. Spacer acquisition and PAM mutation rates are updated at the next strain addition or dilution event or at a preset maximum update interval ($\frac{1}{2}$hr) and used to draw the time of next addition from an exponential distribution.

When an addition event occurs the type of event is drawn with each type's probability being proportional to its calculated rate. We then draw the strain in the population to serve as the base for the new strain, with the probability of choosing each strain proportional to its strain-specific acquisition, mutation, or recombination rate. In the case of spacer acquisition a spacer is drawn with probabilities based on the overall prevalence of each corresponding protospacer in the phage population. In the case of PAM mutation or back mutation a protospacer is drawn uniformly from the chosen strain's genome. In all cases new strains are added at a population size of 100 individuals so that we focus only on strains that are able to establish themselves and neglect drift to speed up computation. Accordingly we set μ_b, μ_p, and μ_q lower than might otherwise be expected (see S2 Text). During simulations we dynamically adjust our rates so as to avoid adding strains already present in the system.

S4 Experimental Methods

Powdered skim milk (Publix) was diluted in distilled water, 10gms/100ml water. The suspension was autoclaved at 110°C for 12 minutes. Three ml of the milk was then put into 13mm x100mm glass tubes. *Streptococcus thermophilus* (DGCC7710) were grown overnight in a broth, LM17 with added calcium (Levin *et al.*, 2013). To initiate the serial transfer cultures, 30 μl of the overnight broth was added to the tubes either alone or with the phage from an LM17 Ca lysate. The initial densities of the bacteria and phage were estimated by serial dilution and plating on LM17Ca agar for the bacteria and with LM17Ca soft agar for the phages (see Levin *et al.* 2013). Each day, the cultures were vortexed to suspend the bacteria and phages (the milk fermented), densities were estimated, and 30 μl of the cultures were transferred to fresh tubes with 3 ml milk. These cultures were serially passaged for the noted number of days, with bacteria and phage densities estimated daily.

To test for bacteriophage immune mutants, periodically, single colonies from the sampling plates were grown up on LM17 and used as lawns to test for their sensitivity to the original phage and the phage in their respective cultures. For the latter, LM17 lysates were made from single plaques taken from the sampled plates. In this way, we were able to test for CRISPR escape mutants. For example, if the bacteria from the culture appeared immune to the original phage, we would then test for its sensitivity to phage from the serial passage culture. In this way, we were able to follow some of the co-evolution that was occurring in the cultures, via the acquisition of new spacers generating host and phage mutants evolving in these cultures, for more details and more extensive consideration of this co-evolution see (Paez-Espino *et al.*, 2013, 2015).

References

Barrangou R, Fremaux C, Deveau H, Richards M, Boyaval P, Moineau S, *et al.* (2007). CRISPR Provides Acquired Resistance Against Viruses in Prokaryotes. *Science* **315**: 1709–1712.

Bohannan BJM, Lenski RE (1997). Effect of resource enrichment on a chemostat community of bacteria and bacteriophage. *Ecology* **78**: 2303–2315.

Bolotin A, Quinquis B, Sorokin A, Ehrlich SD (2005). Clustered regularly interspaced short palindrome repeats (CRISPRs) have spacers of extrachromosomal origin. *Microbiology* **151**: 2551–2561.

Childs LM, Held NL, Young MJ, Whitaker RJ, Weitz JS (2012). Multiscale Model of Crispr-Induced Coevolutionary Dynamics: Diversification at the Interface of Lamarck and Darwin. *Evolution* **66**: 2015–2029.

Deveau H, Barrangou R, Garneau JE, Labonté J, Fremaux C, Boyaval P, *et al.* (2008). Phage Response to CRISPR-Encoded Resistance in Streptococcus thermophilus. *Journal of Bacteriology* **190**: 1390–1400.

Horvath P, Romero DA, Coûté-Monvoisin AC, Richards M, Deveau H, Moineau S, *et al.* (2008). Diversity, Activity, and Evolution of CRISPR Loci in Streptococcus thermophilus. *Journal of Bacteriology* **190**: 1401–1412.

Jiang W, Maniv I, Arain F, Wang Y, Levin BR, Marraffini LA (2013). Dealing with the Evolutionary Downside of CRISPR Immunity: Bacteria and Beneficial Plasmids. *PLoS Genet* **9**: e1003844.

Lévesque C, Duplessis M, Labonté J, Labrie S, Fremaux C, Tremblay D, *et al.* (2005). Genomic Organization and Molecular Analysis of Virulent Bacteriophage 2972 Infecting an Exopolysaccharide-Producing Streptococcus thermophilus Strain. *Applied and Environmental Microbiology* **71**: 4057–4068.

Levin BR, Moineau S, Bushman M, Barrangou R (2013). The Population and Evolutionary Dynamics of Phage and Bacteria with CRISPR–Mediated Immunity. *PLoS Genet* **9**: e1003312.

Paez-Espino D, Morovic W, Sun CL, Thomas BC, Ueda Ki, Stahl B, *et al.* (2013). Strong bias in the bacterial CRISPR elements that confer immunity to phage. *Nature Communications* **4**: 1430.

Paez-Espino D, Sharon I, Morovic W, Stahl B, Thomas BC, Barrangou R, *et al.* (2015). CRISPR immunity drives rapid phage genome evolution in Streptococcus thermophilus. *MBio* **6**: e00262–15.

Wei Y, Terns RM, Terns MP (2015). Cas9 function and host genome sampling in Type II-A CRISPR–Cas adaptation. *Genes & Development* **29**: 356–361.

S5 Tables

	Eq. 1	Eq. 2	Eq. 3	Eq. 4
$\tilde{R}$	A	$\frac{z(\alpha+\mu+w)}{v-\alpha-\mu-w}$	$\frac{1}{2}\left(A-\frac{ev\tilde{U}}{w}-z+\sqrt{4Az+\left(A-\frac{ev\tilde{U}}{w}-z\right)^2}\right)$	$\frac{zw}{v-w}$
$\tilde{D}$	0	$(\phi_u\beta-1)\tilde{U}-\frac{w}{\delta}$	0	0
$\tilde{U}$	0	$\frac{1}{\phi_u\beta}\left(\frac{w(A-\tilde{R})(z+\tilde{R})}{ev\tilde{R}}+\frac{w}{\delta}\right)$	$\frac{w}{\delta(\phi\beta-1)}$	$\frac{w(A-\tilde{R})(z+\tilde{R})}{ev\tilde{R}}$
$\tilde{P}$	0	$\frac{1}{\phi_u\delta}\left(\frac{v\tilde{R}}{z+\tilde{R}}-w+\mu\left(\frac{\tilde{D}}{\tilde{U}}\right)\right)$	$\frac{1}{\phi\delta}\left(\frac{v\tilde{R}}{z+\tilde{R}}-w\right)$	0

Supplementary Table 1: Equilibrium of general model without coevolution. Equilibria for the autoimmunity/locus-loss model where $\mu > 0$ and $\alpha > 0$. Not all substitutions have been made here in the interest of readability, but equilibrium values can be easily computed using the above expressions. The stability of these equilibria can be assessed by linearizing our system around them (i.e., taking the Jacobian) as described in Supplementary Text S3.

	Spacer ID																					
Transfer	A	B	C	D	E	F	G	H	I	J	K	L	M	N	O	P	Q	R	S	T	U	V
1	1	1	1	1																		
2			1	1	1	1																
3			1	2		1	1															
4								1														
5					2	2	1		1	1												
11				1	1		2				1	1	1									
15				1		1							2	2	1							
25					5				1							1	1					
35					1		2											1	2			
40							2							2						3	1	1

Supplementary Table 2: Spacer dynamics for long term coevolution experiment (Experiment 1). Spacers dynamics in the CRISPR1 locus for serial transfer experiment 1. Each letter corresponds to a unique spacer sequence. All sampled sequences shown with the number of times observed at each timepoint.

S6 Figures

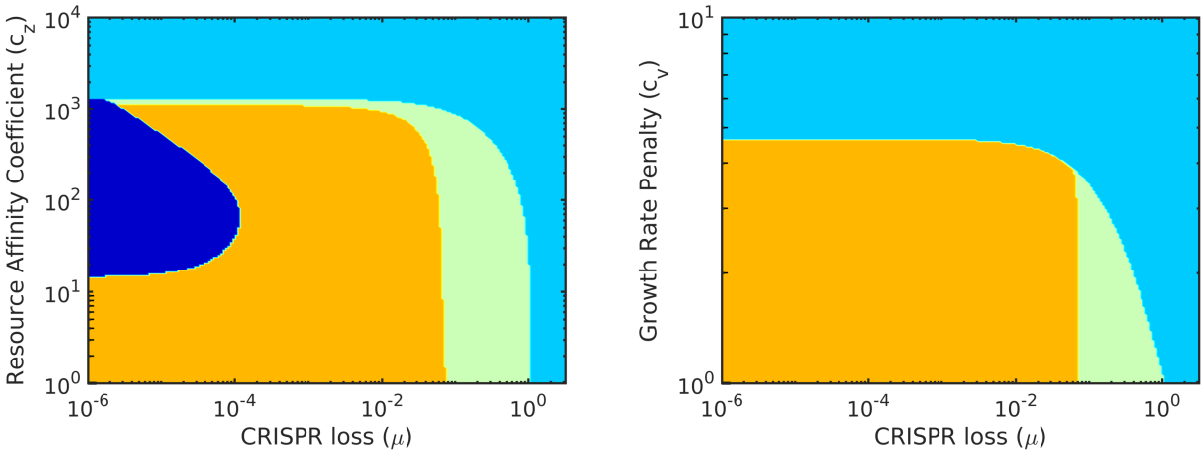

(a) $c_v = 1$ **(b)** $c_z = 1$

Supplementary Figure 1: Equilibria with alternative costs of immunity. Model behavior under variations in the immune system loss rate and (a) resource affinity coefficient or (b) growth rate penalty. Equilibria derived from our equations in Supplementary Text S1 are shown where orange indicates a stable equilibrium with all populations coexisting and defended host dominating phage populations, green indicates that all populations coexist but phages dominate, light blue indicates that defended bacteria have gone extinct but phages and undefended bacteria coexist, and dark blue indicates that there is no stable equilibrium. We neglect coevolution and innate immunity in this analysis ($\phi_u = 1$, $\phi_d = 0$) and do not consider the effects of autoimmunity ($\alpha = 0$).

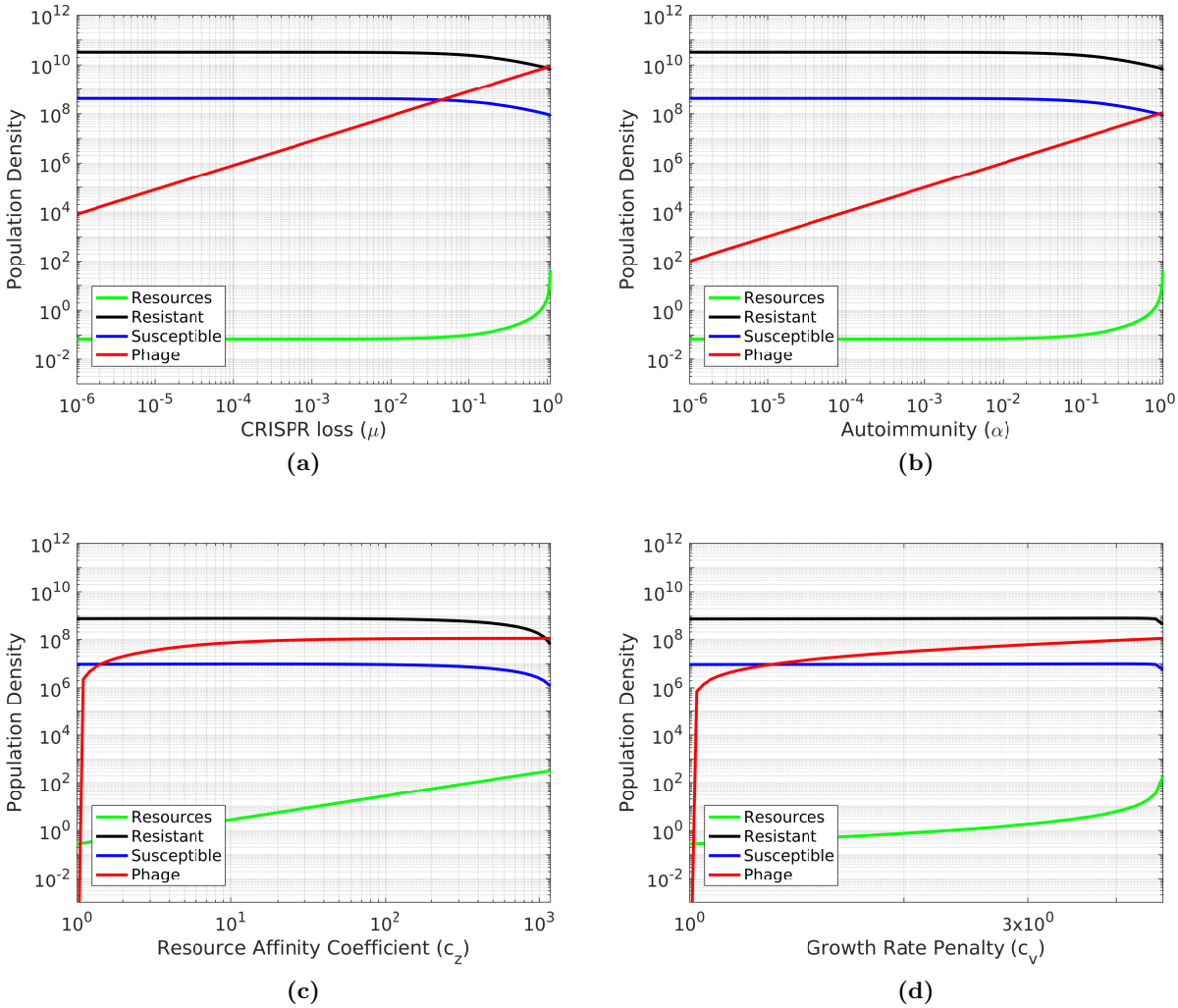

Supplementary Figure 2: Equilibria with each coexistence mechanism in isolation. Behavior of coexistence equilibrium when (a) there is only CRISPR loss without autoimmunity, (b) there is only autoimmunity without CRISPR loss, (c) there is only a cost applied to resource affinity (Supplementary Text S1), and (d) there is only a cost applied to maximum growth rate (Supplementary Text S1). Notice that immune loss and autoimmune mechanisms essentially act in the same manner, except that the loss mechanism produces a larger phage population by flushing extra susceptible bacteria into the system. This is consistent with theoretical results showing that increasing resource availability in a host-phage system increases phage rather than host populations (Bohannan and Lenski, 1997). The upper bound of the x-axis in (a-d) represents the upper limit of the cost of immunity, above which coexistence will not occur because immune host cannot survive.

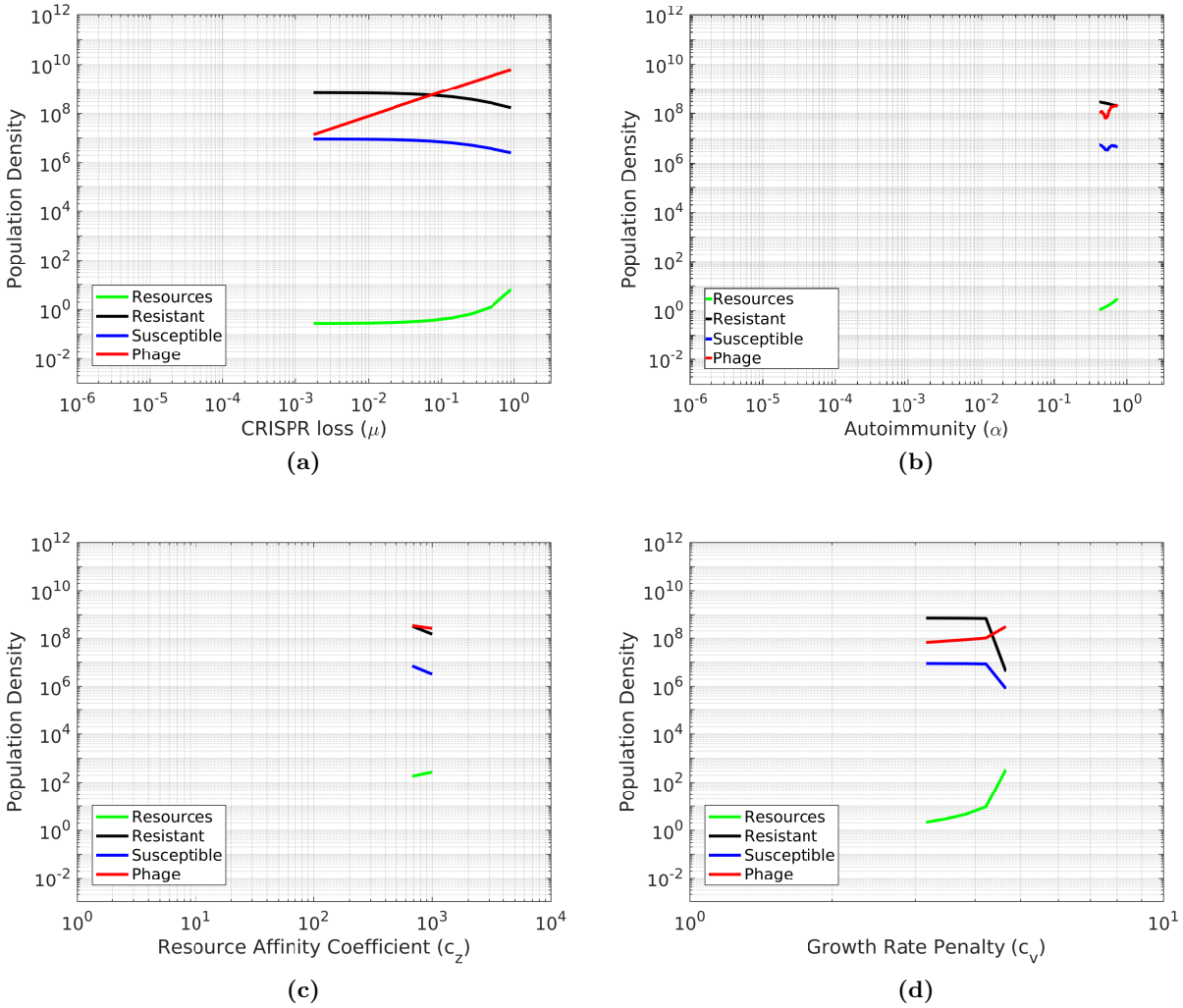

Supplementary Figure 3: Numerical solutions to model at 80 days with realistic initial conditions. Numerical solutions to the alternative cost model (Supplementary Text S1) at 80 days using realistic initial conditions more specific to the experimental setup ($R(0) = 350$, $D(0) = 10^6$, $U(0) = 100$, $P(0) = 10^6$). Results only shown for cases in which all three populations remained extant. Results in each panel correspond to each mechanism in isolation.

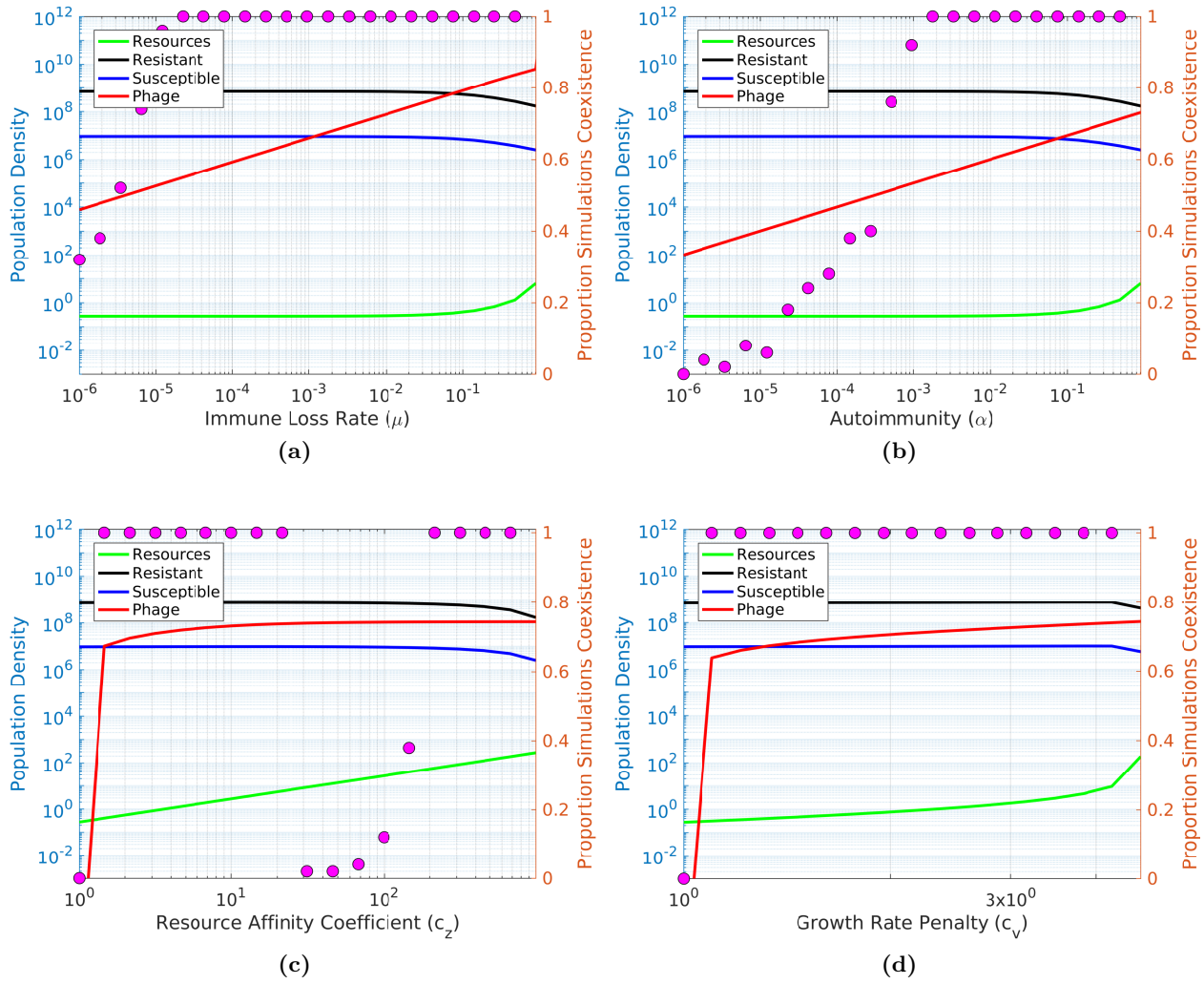

Supplementary Figure 4: Simulations of perturbed starting conditions (small perturbations). We find numerical solutions to the alternative cost model (Supplementary Text S1) at 80 days with starting conditions $(X(0) = [R(0), D(0), U(0), P(0)])$ perturbed by a proportion of the equilibrium condition $X(0) = \tilde{X}(1 + \gamma Y)$ where $Y \sim U[0, 1]$ and $\tilde{X}$ signifies an equilibrium value to explore how robust the equilibria are to starting conditions. We ran 50 simulations for each condition. We let $\gamma = 0.1$. Lines correspond to the left axis and purple dots correspond to the right axis. Results in each panel correspond to each mechanism in isolation.

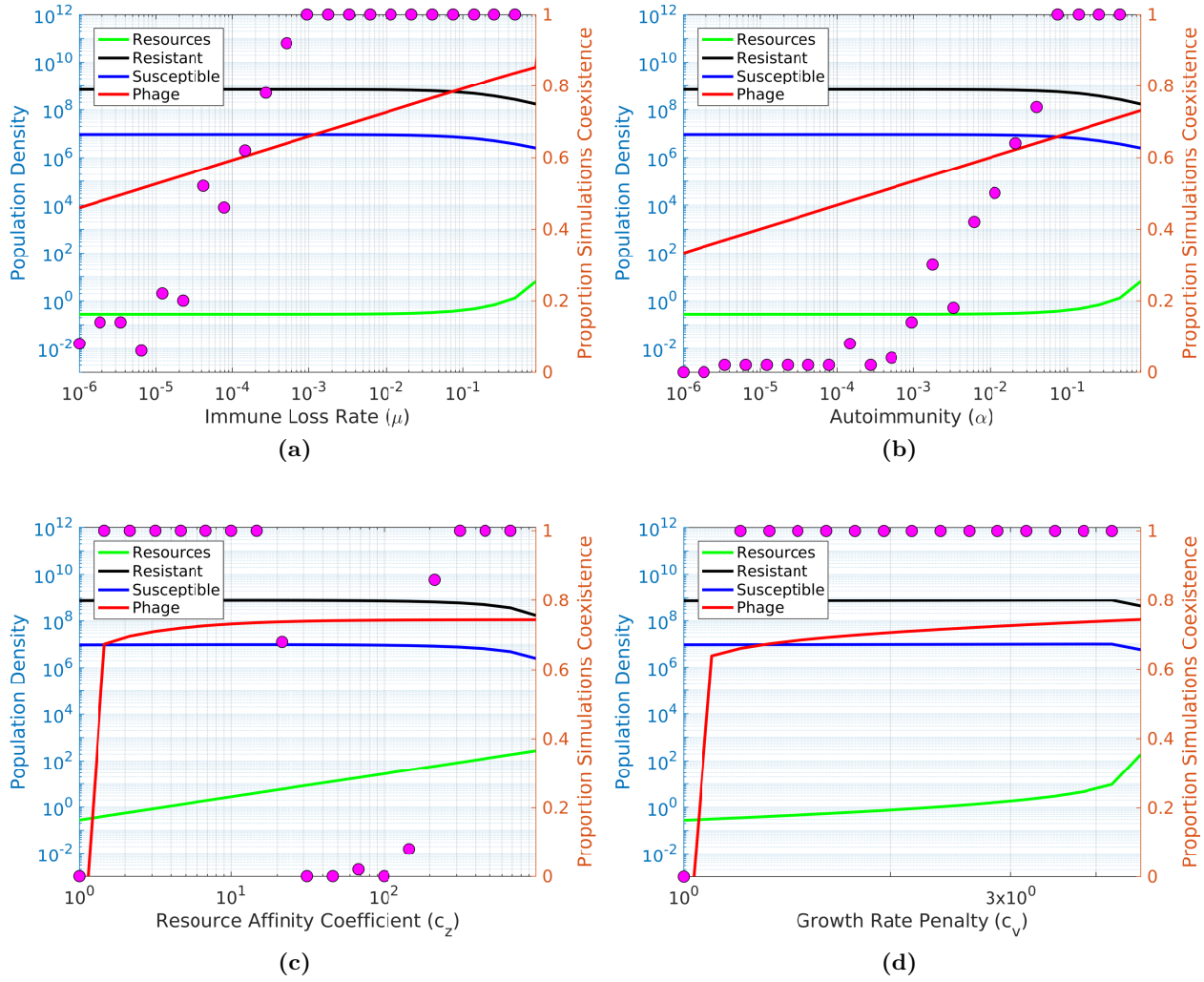

Supplementary Figure 5: Simulations of perturbed starting conditions (intermediate perturbations). We find numerical solutions to the alternative cost model (Supplementary Text S1) at 80 days with starting conditions $(X(0) = [R(0), D(0), U(0), P(0)])$ perturbed by a proportion of the equilibrium condition $X(0) = \tilde{X}(1 + \gamma Y)$ where $Y \sim U[0, 1]$ and $\tilde{X}$ signifies an equilibrium value to explore how robust the equilibria are to starting conditions. We ran 50 simulations for each condition. We let $\gamma = 1$. Lines correspond to the left axis and purple dots correspond to the right axis. Results in each panel correspond to each mechanism in isolation.

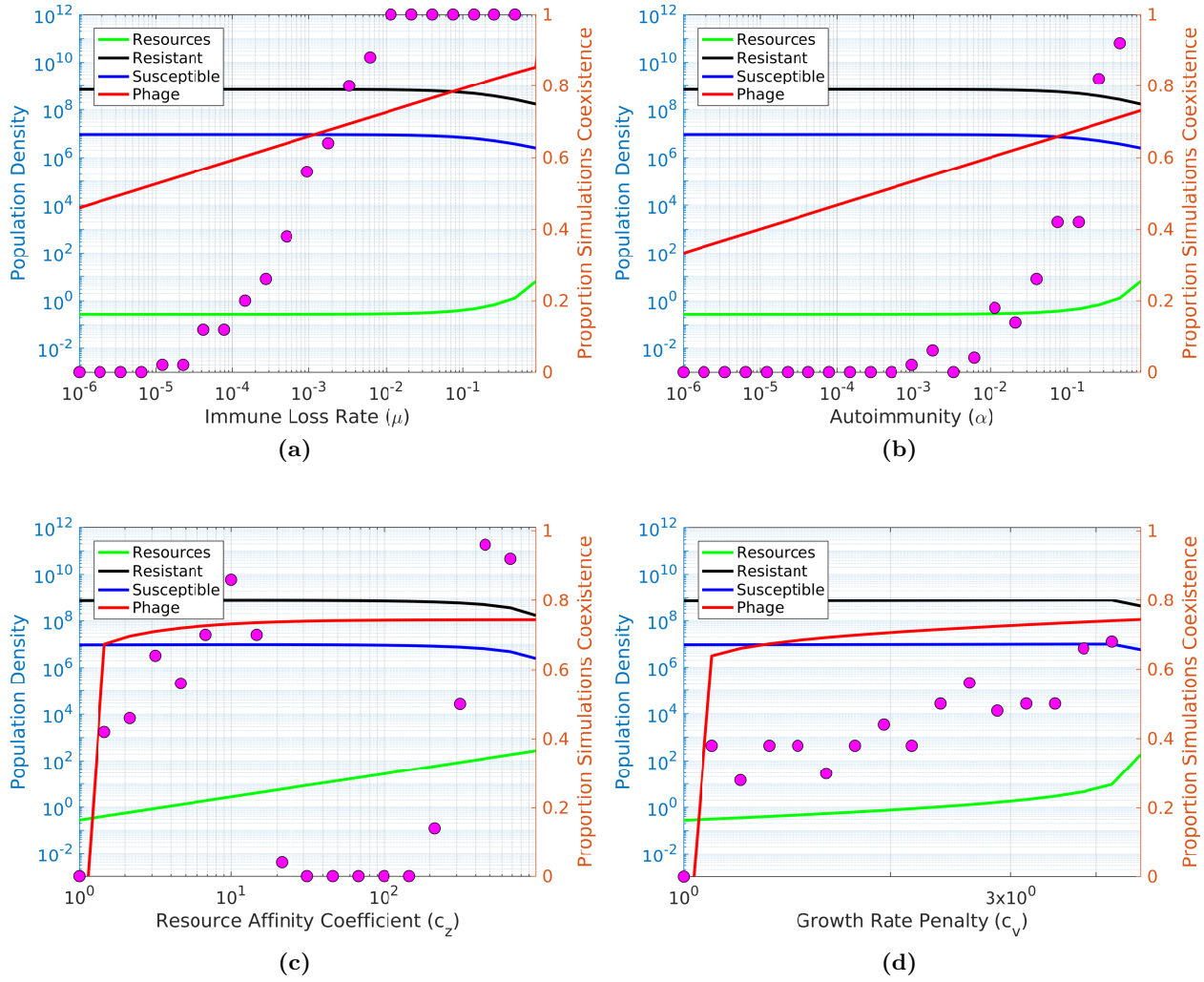

Supplementary Figure 6: Simulations of perturbed starting conditions (large perturbations). We find numerical solutions to the alternative cost model (Supplementary Text S1) at 80 days with starting conditions $(X(0) = [R(0), D(0), U(0), P(0)])$ perturbed by a proportion of the equilibrium condition $X(0) = \tilde{X}(1 + \gamma Y)$ where $Y \sim U[0, 1]$ and $\tilde{X}$ signifies an equilibrium value to explore how robust the equilibria are to starting conditions. We ran 50 simulations for each condition. We let $\gamma = 10$. Lines correspond to the left axis and purple dots correspond to the right axis. Results in each panel correspond to each mechanism in isolation.

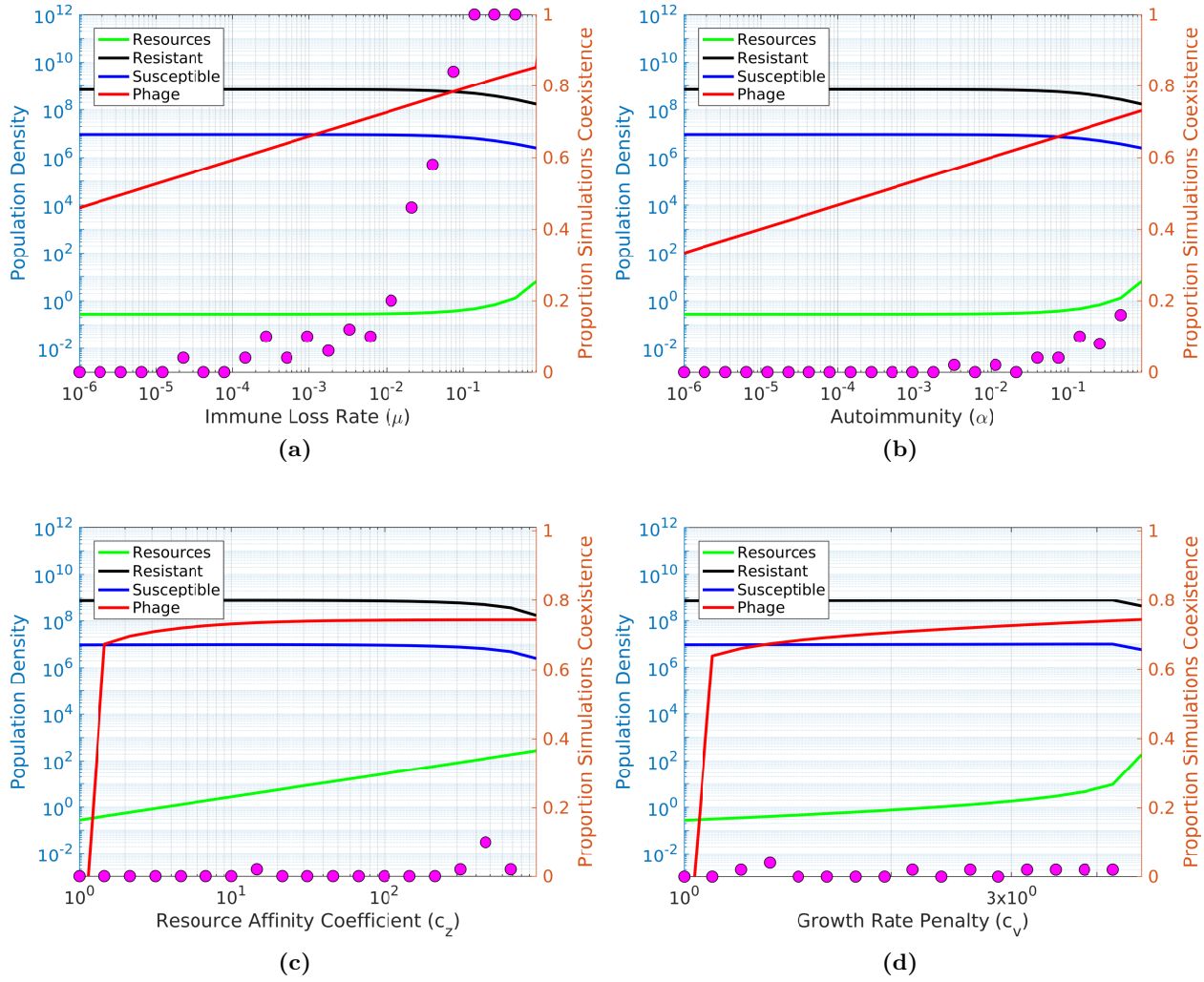

Supplementary Figure 7: Simulations of perturbed starting conditions (very large perturbations). We find numerical solutions to the alternative cost model (Supplementary Text S1) at 80 days with starting conditions $(X(0) = [R(0), D(0), U(0), P(0)])$ perturbed by a proportion of the equilibrium condition $X(0) = \tilde{X}(1 + \gamma Y)$ where $Y \sim U[0, 1]$ and $\tilde{X}$ signifies an equilibrium value to explore how robust the equilibria are to starting conditions. We ran 50 simulations for each condition. We let $\gamma = 100$. Lines correspond to the left axis and purple dots correspond to the right axis. Results in each panel correspond to each mechanism in isolation.

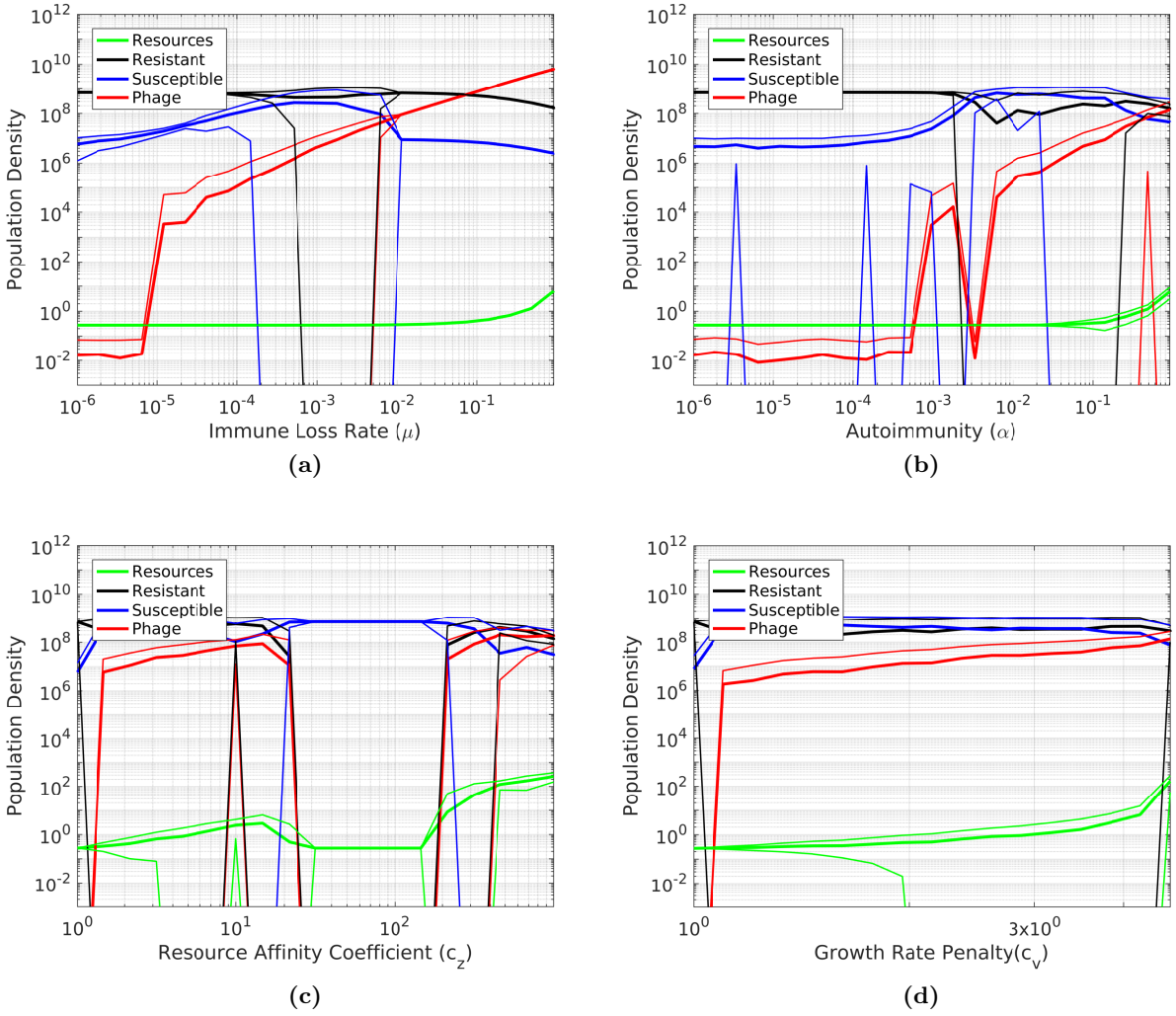

Supplementary Figure 8: Mean population size with perturbed starting conditions (intermediate perturbations). We find numerical solutions to the alternative cost model (Supplementary Text S1) at 80 days with starting conditions ($X(0) = [R(0), D(0), U(0), P(0)]$) perturbed by a proportion of the equilibrium condition $X(0) = \tilde{X}(1 + \gamma Y)$ where $Y \sim U[0, 1]$ and $\tilde{X}$ signifies an equilibrium value to explore how robust the equilibria are to starting conditions. We ran 50 simulations for each condition. We let $\gamma = 10$. Mean population across all simulations (including cases of phage or host extinction) shown by bold line and two standard deviations away from the mean are represented by the thin lines. Results in each panel correspond to each mechanism in isolation.

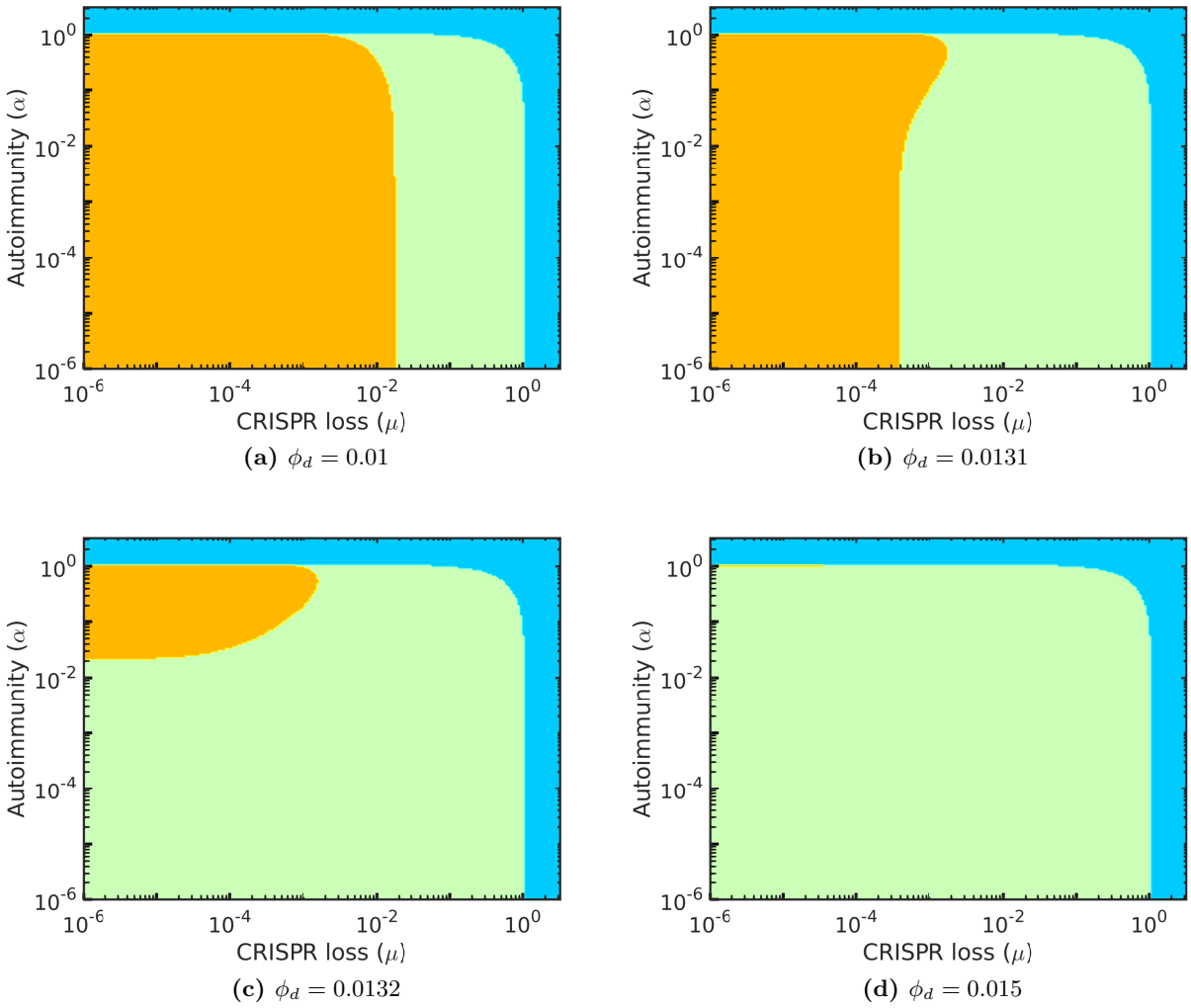

(a) $\phi_d = 0.01$ **(b)** $\phi_d = 0.0131$

(c) $\phi_d = 0.0132$ **(d)** $\phi_d = 0.015$

Supplementary Figure 9: Phase diagram of general model with phage coevolution. Phase diagrams of simple coevolutionary model behavior under variations in the rates of autoimmunity (α) and CRISPR system loss (μ) over various coevolutionary scenarios (ϕ_d). Values of ϕ_d were chosen so as to demonstrate the rapid shift that occurs from host to phage dominated equilibrium as the infected fraction of defended host increases. Orange indicates a stable equilibrium with all populations coexisting and defended host dominating phage populations, green indicates that all populations coexist but phages dominate, and blue indicates that defended bacteria have gone extinct but phages and undefended bacteria coexist.

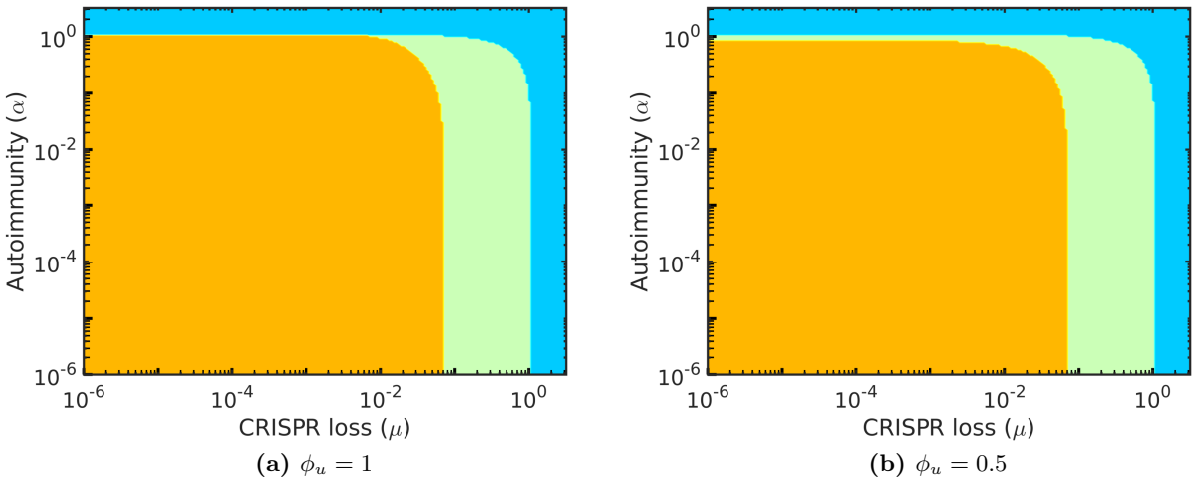

(a) $\phi_u = 1$ **(b)** $\phi_u = 0.5$

(c) $\phi_u = 0.1$ **(d)** $\phi_u = 0.05$

Supplementary Figure 10: Phase diagram of general model with innate immunity. Phase diagram of model behavior under variations in the rates of autoimmunity (α) and CRISPR system loss (μ) for different values of (ϕ_u). Orange indicates a stable equilibrium with all populations coexisting and defended host dominating phage populations, green indicates that all populations coexist but phages dominate, and blue indicates that defended bacteria have gone extinct but phages and undefended bacteria coexist.

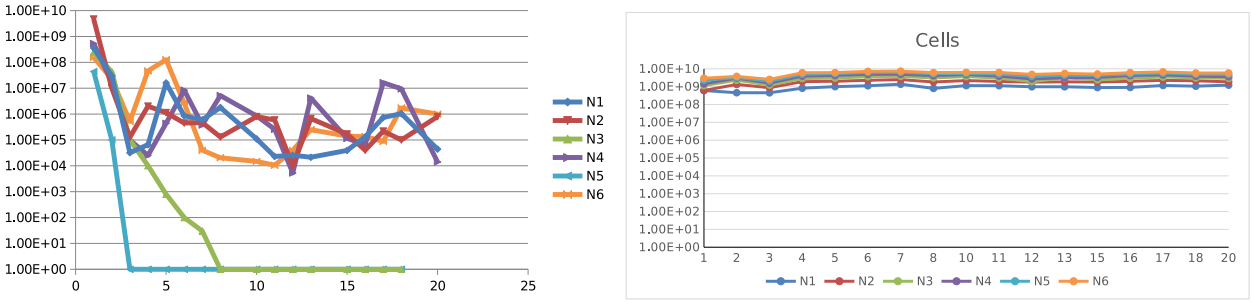

(a) Phage **(b)** Bacteria

Supplementary Figure 11: Replicate serial transfer experiments. Densities of (a) phage and (b) bacteria measured daily at serial transfer. All replicate experiments start with the same conditions and strains as in the main text.

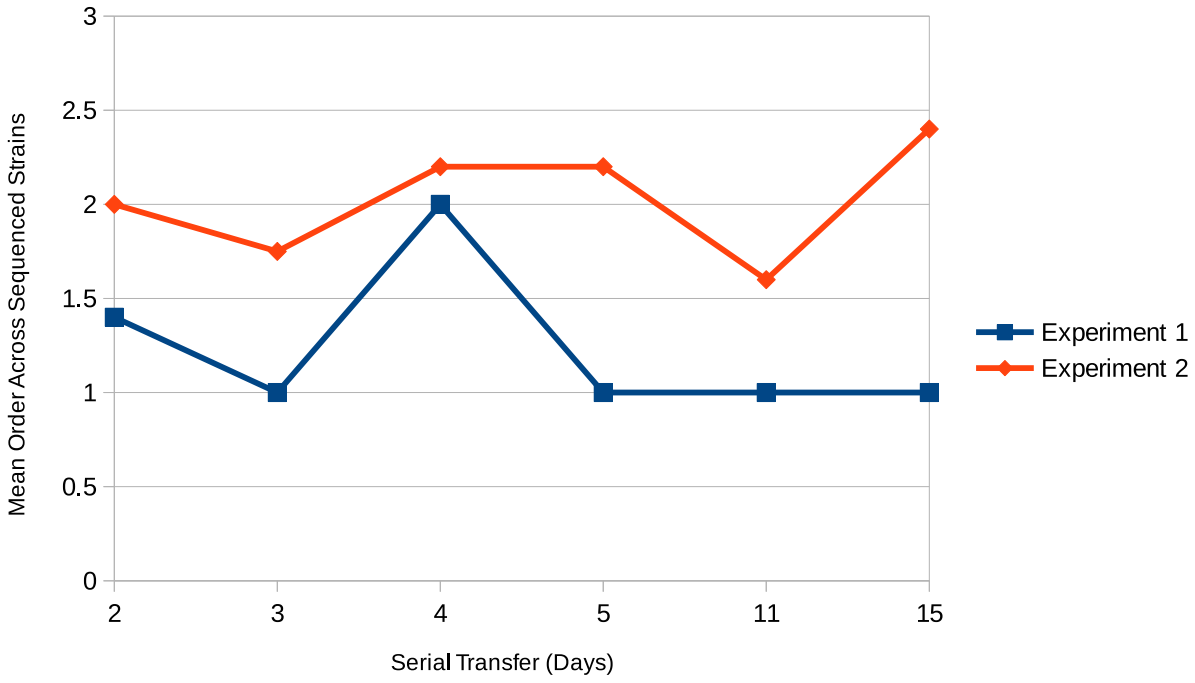

Supplementary Figure 12: Mean sequenced order of host over time in serial transfer experiments 1 and 2. Sum over CRISPR1 and CRISPR3 loci.

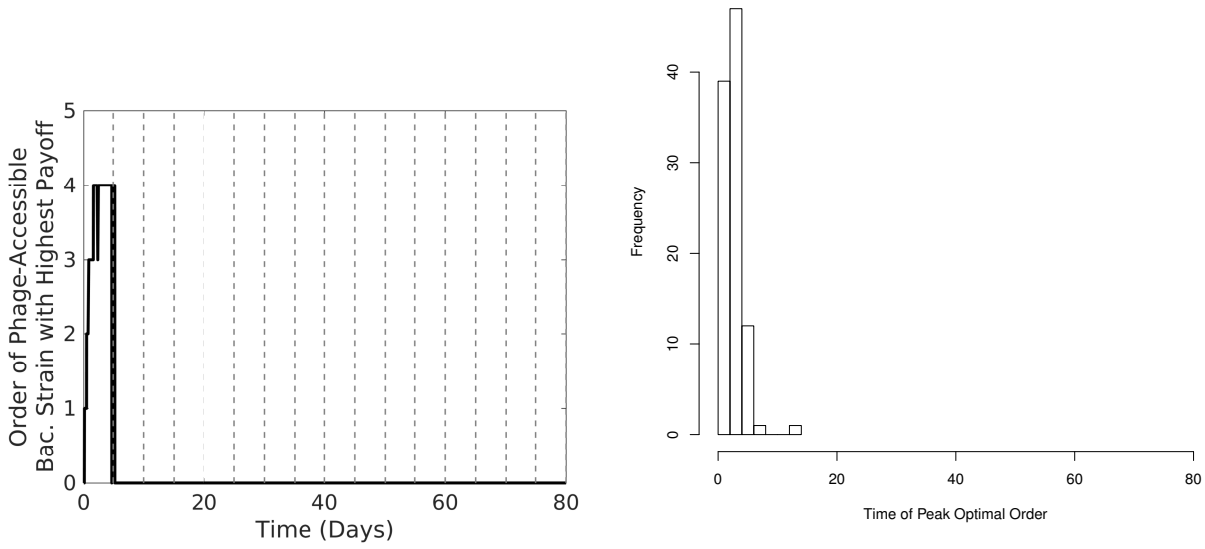

(a) **(b)**

Supplementary Figure 13: Optimal host order for phages to infect over time. The optimal host strain that is either currently infected by a phage strain or one PAM mutation away from being infected. Optimality is defined in terms of population size times the burst size of the phage strain that does or could infect that strain, so that the balance between abundant host and mutation cost is taken into account. In (a) we track the order of the "best" available host strain at any given point in a single example simulation (Fig 22), and in (b) look at the timing of the peak optimal order across 100 simulations (Main text fig 4, $\mu_q = 5 \times 10^{-9}$). Note that after the initial arms race dynamic the best available host strain is the CRISPR-lacking host in all simulations. The order of the best host strain peaks early on in all simulations and then drops to zero (CRISPR-lacking), signifying an early end to the arms race between host and phage.

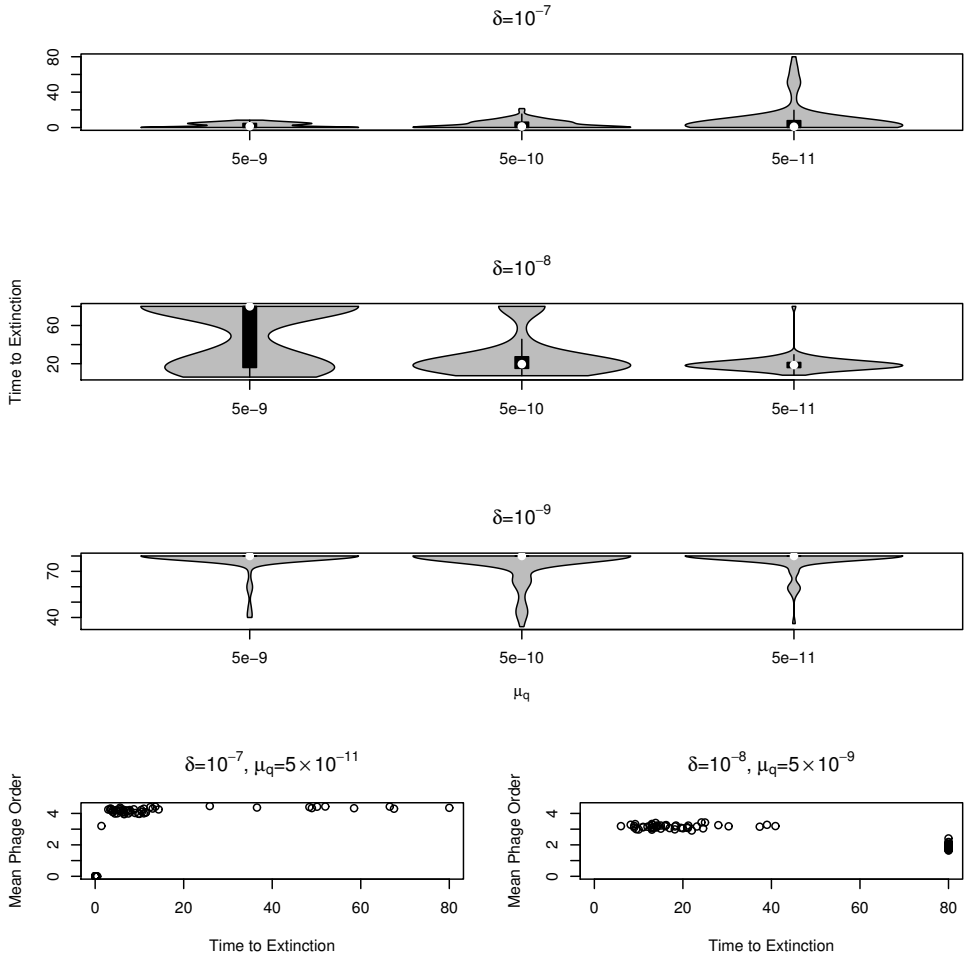

Supplementary Figure 14: Effect on simulations of varied phage adsorption rates. Adsorption rate has a profound effect on the outcome of host-phage interactions. At a high adsorption rate ($\delta = 10^{-7}$) either phages or bacteria tend to go extinct early on in the simulation, and phages are able to drive their host extinct approximately 50% of the time (49/100 simulations for all back-mutation rates). We see a reversed relationship of time to extinction with μ_q from our base adsorption rate ($\delta = 10^{-8}$, Main text fig 4), although in general at a very high adsorption rate few simulations demonstrate long-term coexistence as phage consume all host early on. This suggests that the costs associated with PAM mutations are required to keep phage growth rate low enough to prevent overconsumption of host, and indeed upon closer examination of individual simulations it is clear that back mutations to lower phage orders precipitate phage collapse. In the lowest panel we demonstrate that coexistence in the long term at high δ is associated with a high mean phage order over the course of a simulation, while the opposite is true of our typical intermediate δ. At a low adsorption rate ($\delta = 10^{-9}$) we see populations coexisting until the 80 day mark (max simulation length) in almost all simulations.

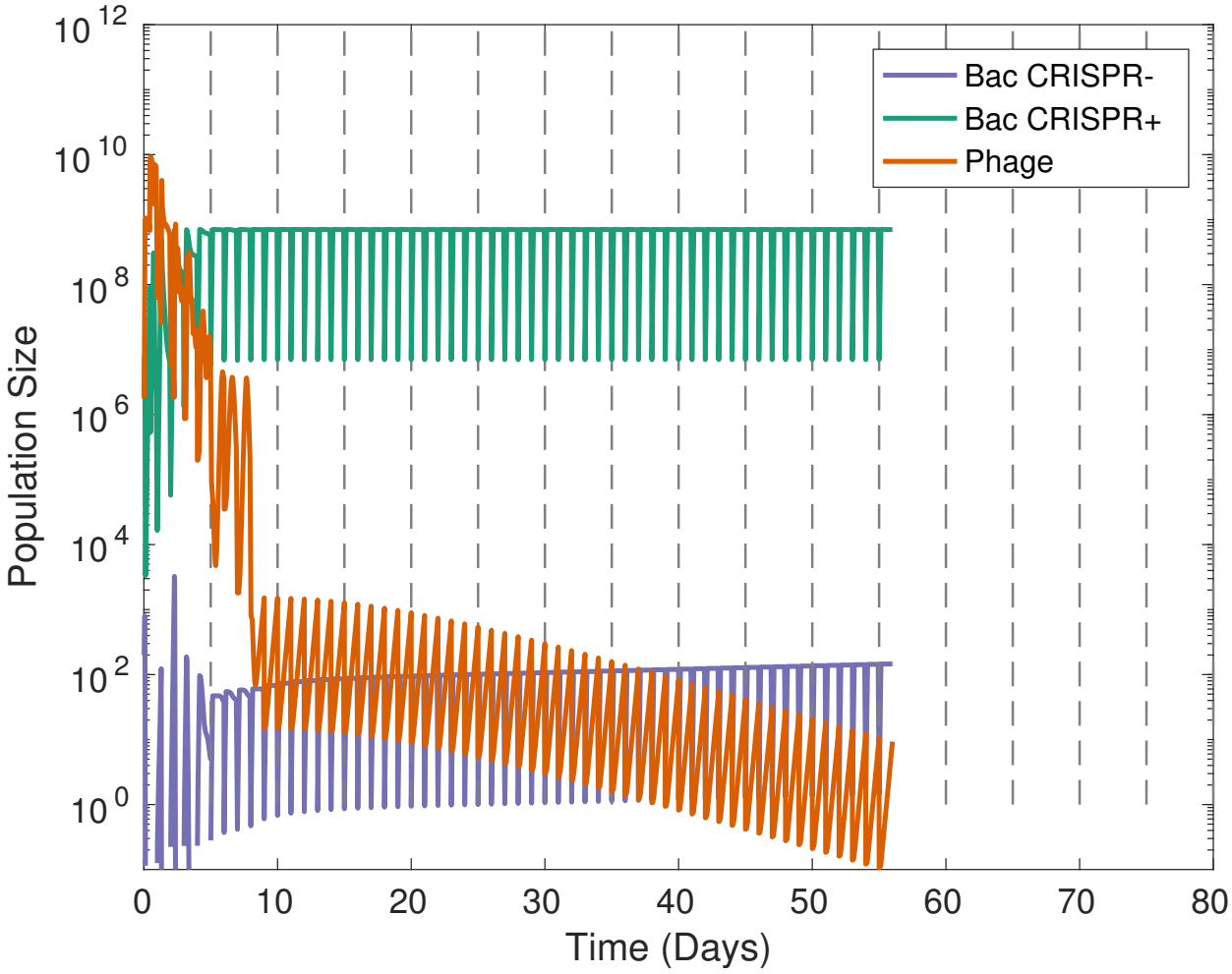

Supplementary Figure 15: Representative simulation with a floor on the susceptible host population and high autoimmunity. We let $B_s > 1 \, \forall t$ and $\alpha = 5 \times 10^{-4}$.

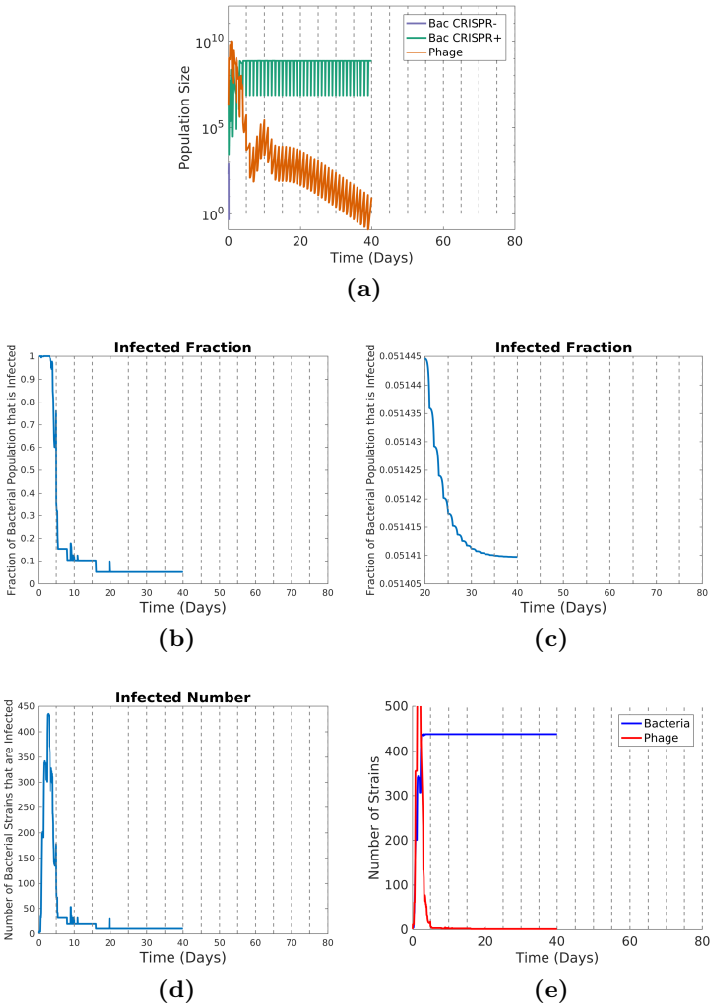

Supplementary Figure 16: Transient phage survival at low density Example of low-level phage persistence due to slow evolutionary dynamics. Here we see that (a) in the absence of the constant production of susceptible bacteria by CRISPR-enabled strains (i.e., $\mu = 0$) phages are still able to paradoxically persist despite a clear advantage to bacteria in the arms race and an absence of other sustaining mechanisms. In (b) a small fraction of the CRISPR enabled bacterial population is maintained that lacks spacers towards the infecting phages and in (c) we zoom in to show that this population is declining due to this infection, but extremely slowly, implying this coexistence is not stable in the long term. The number of bacterial strains that can be infected by phages over time is shown in (d), and (e) shows how the richness of phage and bacterial strains changes over time. Note that although the number of bacterial strains increases asymptotically, after an initial spike the number of strains that can be infected by phages drops dramatically to the single digits. This keeps the overall phage population growth constrained (balanced by adsorption to immune bacteria). In fact, over time phage act to suppress their own growth by negatively infecting the competitiveness of their host (although this effect is so small that phages can persist for an extended period of time seemingly stably). What looks flat is actually monotonically decreasing. All parameters as in Main Text Table 3 and $\alpha = 0$.

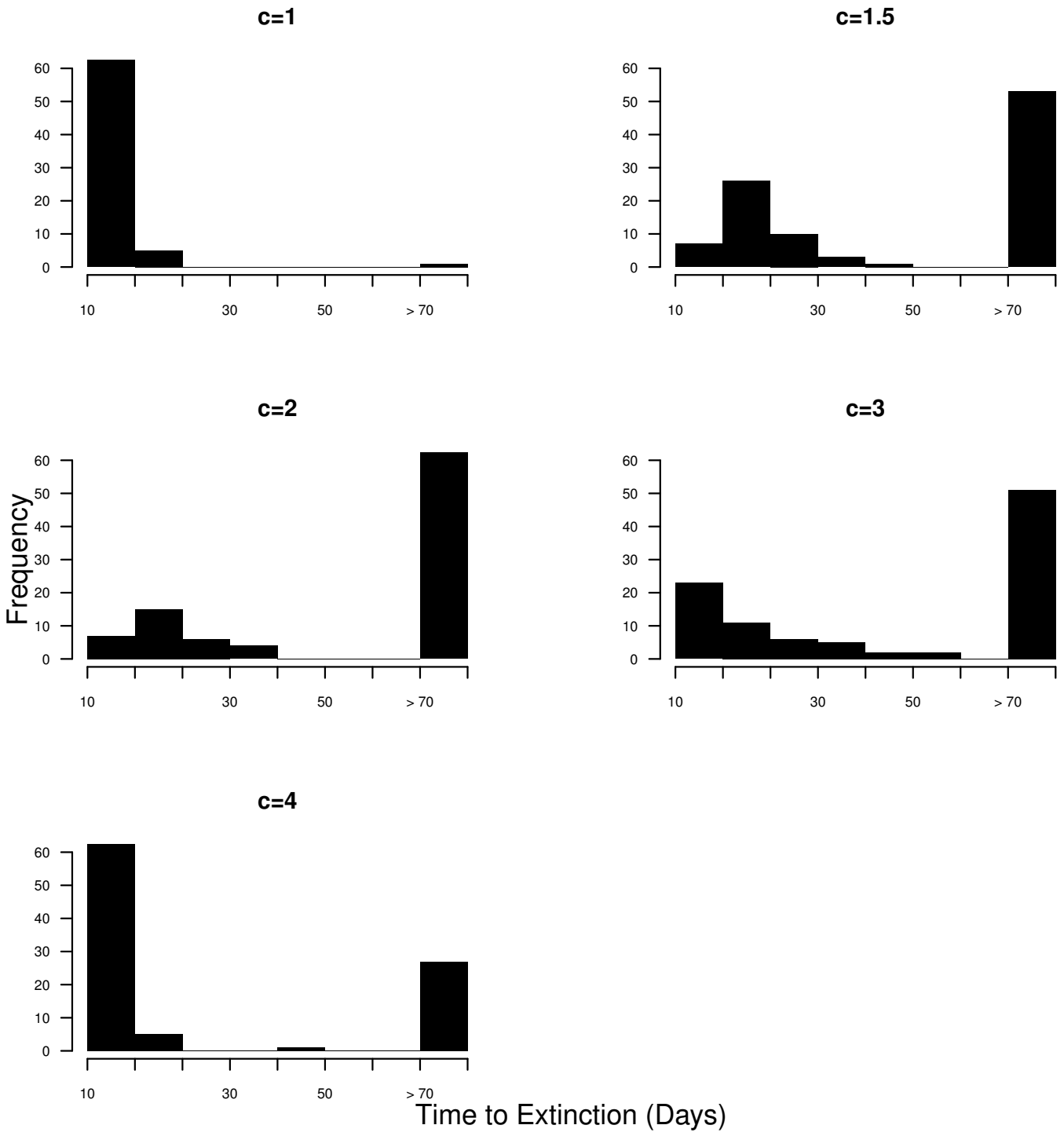

Supplementary Figure 17: Effect of changes in PAM mutation cost (c). Distribution of phage extinction times in bacterial-dominated cultures with different costs on PAM mutation in phage (c). The peak at 80 corresponds to stable coexistence (simulations ran for a maximum of 80 days). These results of for a locus-loss mechanism only ($\mu_L = 5 \times 10^{-4}$, $\alpha = 0$).

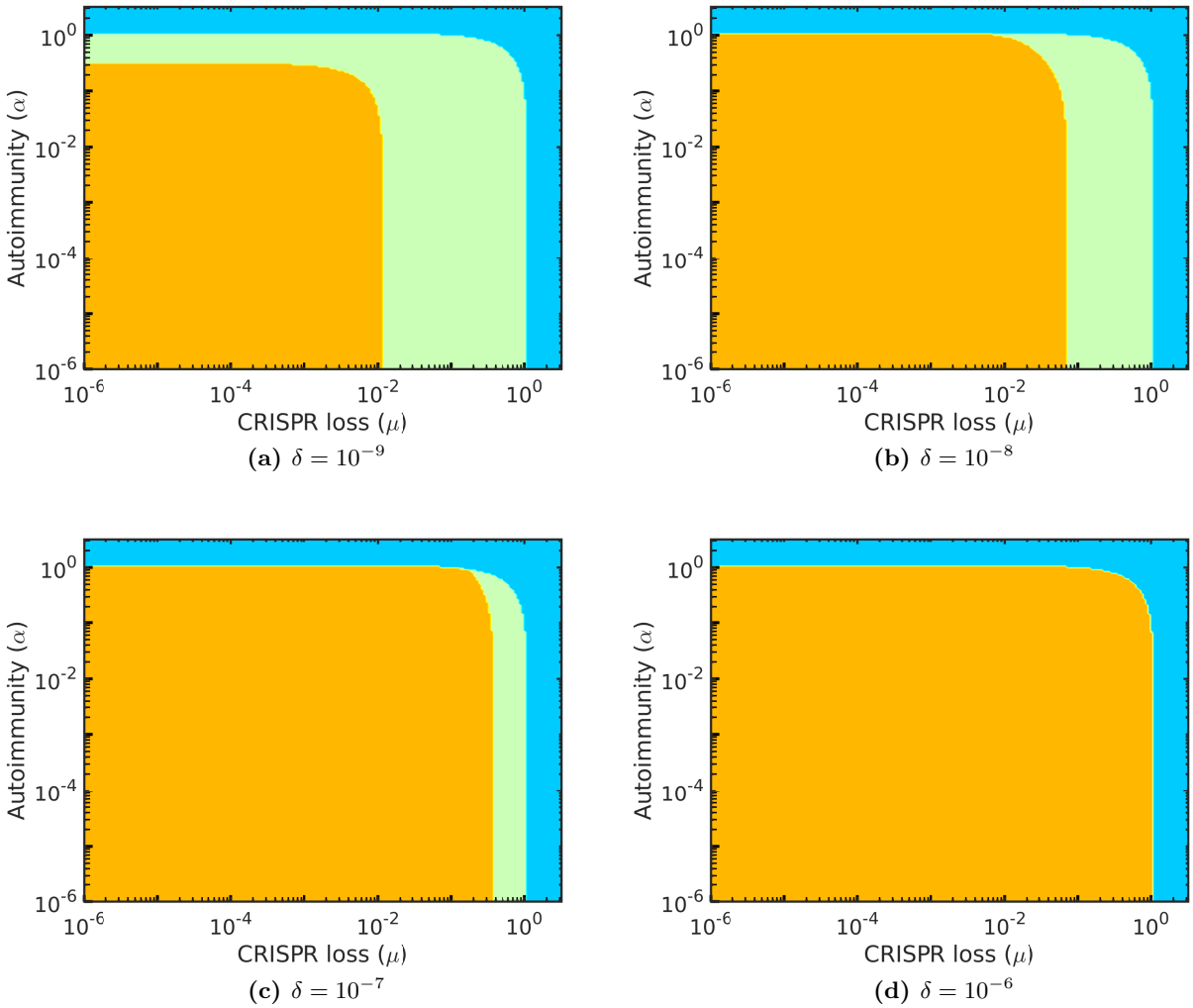

(a) $\delta = 10^{-9}$ **(b)** $\delta = 10^{-8}$

(c) $\delta = 10^{-7}$ **(d)** $\delta = 10^{-6}$

Supplementary Figure 18: Phase diagram of general model with phage coevolution. Phase diagrams of model behavior without coevolution or other forms of immunity ($\phi_d = 0$, $\phi_u = 1$) under variations in the rates of autoimmunity (α) and CRISPR system loss (μ) over various adsorption rates (δ). Orange indicates a stable equilibrium with all populations coexisting and defended host dominating phage populations, green indicates that all populations coexist but phages dominate, and blue indicates that defended bacteria have gone extinct but phages and undefended bacteria coexist. There is an apparent increase in the area of the coexistence region in which host dominate as adsorption rate increases.

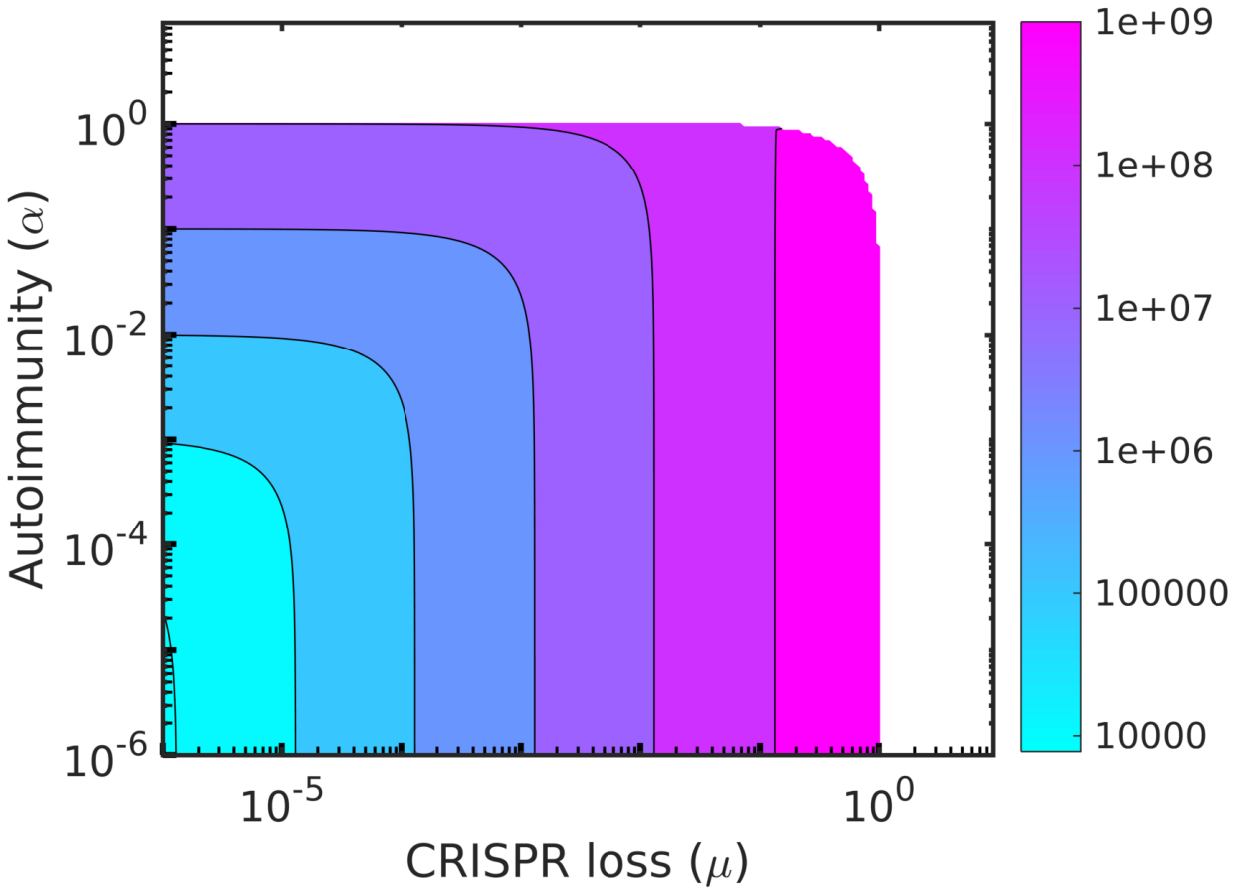

Supplementary Figure 19: Equilibrium phage population during coexistence. Equilibrium population of phages when there is full coexistence over a range of α and μ_L values for our general model without coevolution ($\phi_u = 1$, $\phi_d = 0$).

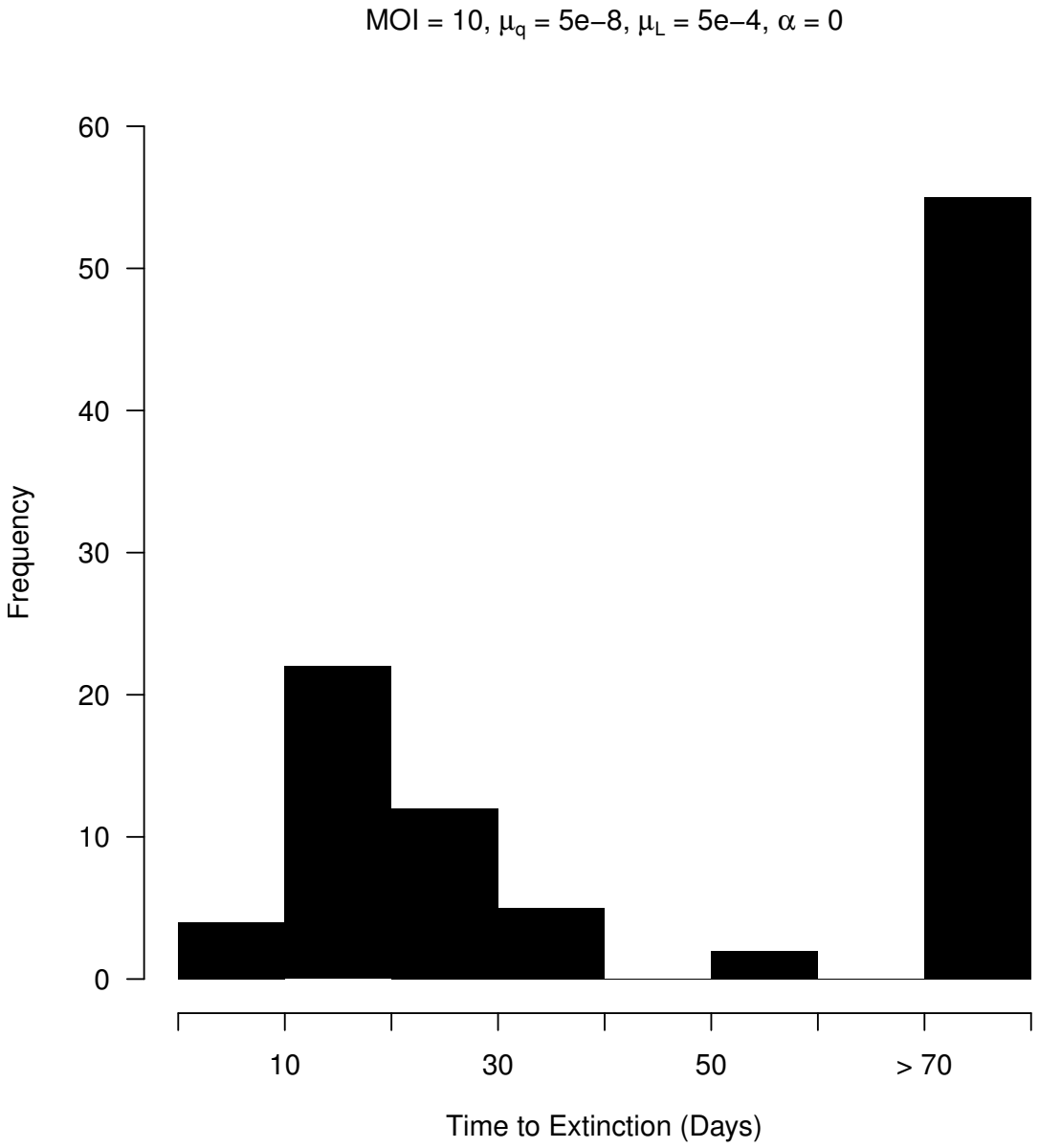

Supplementary Figure 20: Distribution of phage extinction times in bacterial-dominated cultures with an MOI of 10. The peak at 80 corresponds to what we call stable coexistence (simulations ran for a maximum of 80 days).

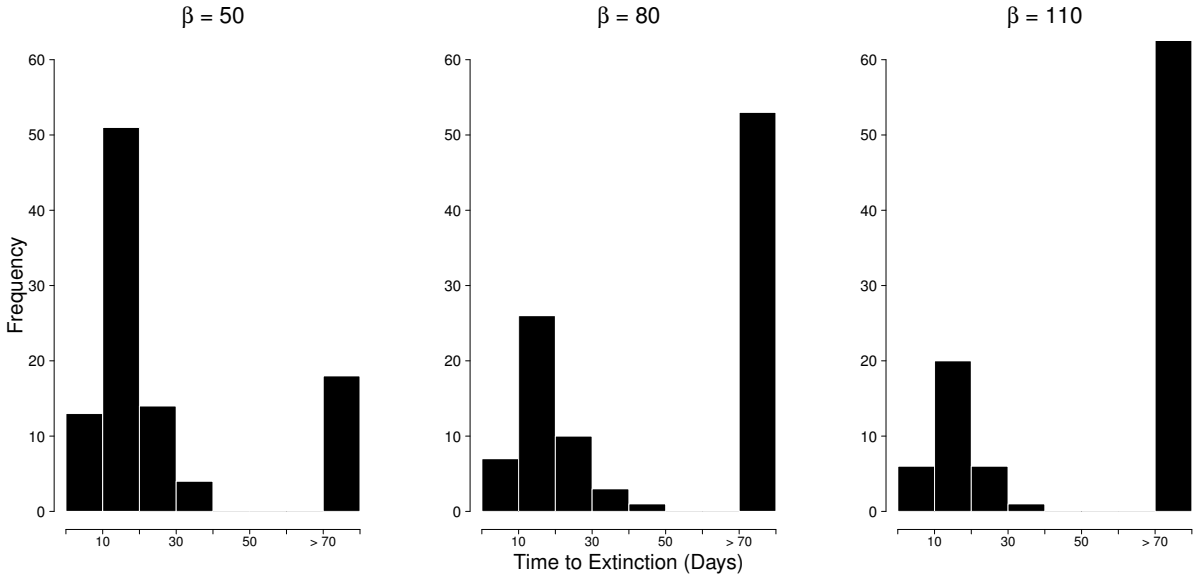

Supplementary Figure 21: Distributions of phage extinction times in bacterial-dominated cultures with various burst sizes. The peak at 80 corresponds to what we call stable coexistence (simulations ran for a maximum of 80 days).

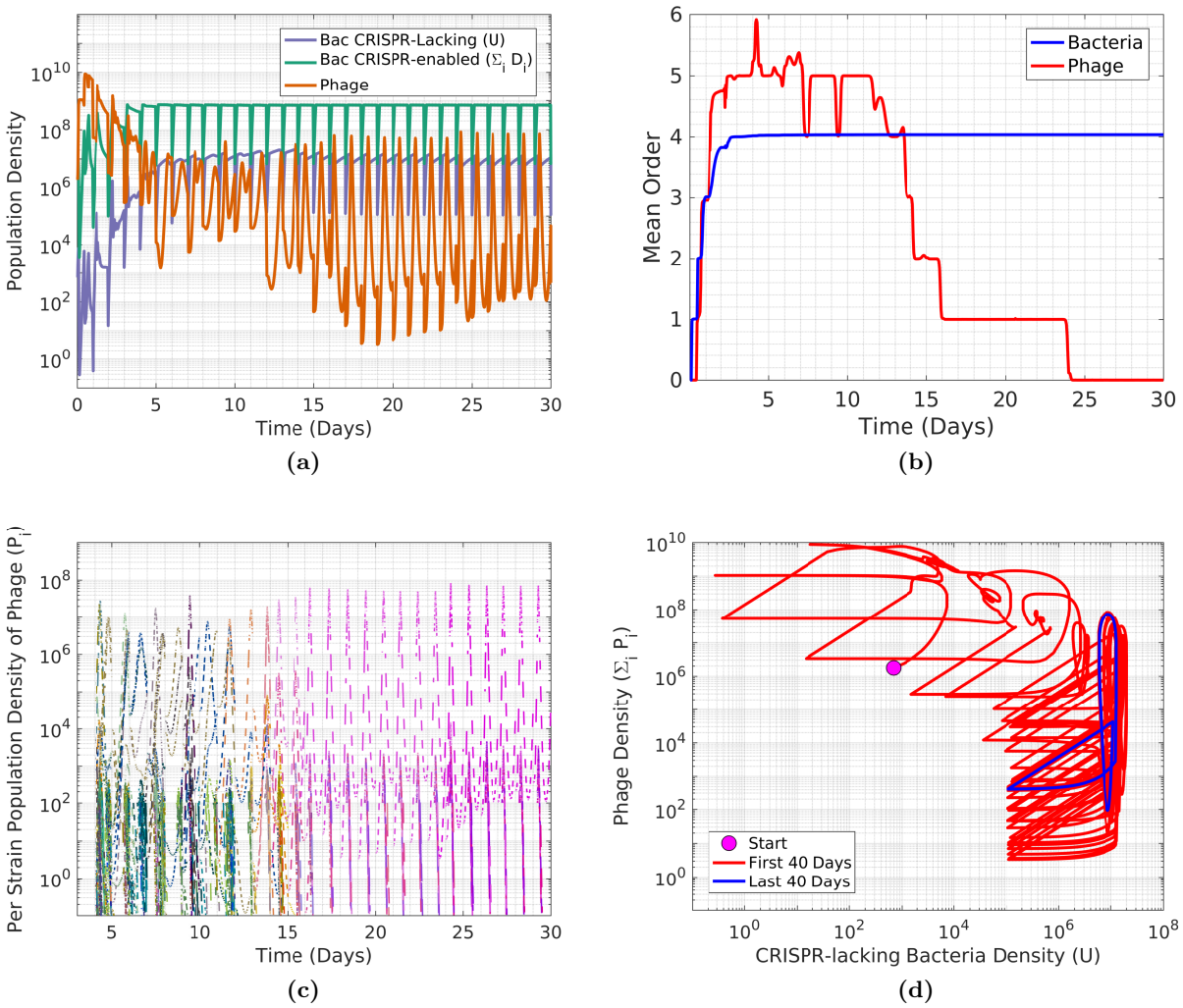

Supplementary Figure 22: Representative example of a simulation demonstrating stable coexistence under a loss mechanism ($\mu_L = 5 \times 10^{-4}$, $\alpha = 0$, $\mu_q = 5 \times 10^{-9}$) In (a) we show the archetypal shift from phage-dominance during an initial arms race to unstable host-dominated coexistence where fluctuating selection dynamics are observed to stable host-dominated predator-prey cycling of phages and CRISPR-lacking hosts as seen in (d) where evolution ceases to occur. In (b) we see that a drop in mean phage order leads to stable cycling and in (c) that this corresponds to a single phage strain becoming dominant after previous cycling of strains. This corresponds to a shift away from fluctuating selection dynamics. In (c) the colors specify different phage strains.